

Cite this: *Nanoscale Adv.*, 2022, 4, 1119

# Nanoporous membrane fabrication by nanoimprint lithography for nanoparticle sieving

Ainur Sabirova,<sup>a</sup> Camelia F. Florica,<sup>b</sup> Florencio Pisig, Jr.,<sup>b</sup> Ahad Syed,<sup>b</sup> Ulrich Buttner,<sup>b</sup> Xiang Li<sup>a</sup> and Suzana P. Nunes<sup>✉</sup><sup>\*,a</sup>

An isoporous membrane with strictly controlled pore size, shape and distribution could provide an efficient, precise and mild sieving of particles in nanotechnology and biomedical applications. However there is a lack of highly porous polymeric membranes combining isoporosity and high permeance in the range below 500 nm. Track-etched membranes are practically the only commercial option. Membranes prepared by phase inversion typically have a broad pore size distribution. Most nanofabrication methods have limited the preparation of membranes with pores in the micrometer range. In this work, we present a nanotechnology-based fabrication methodology to manufacture a stable and flexible nanoporous polymeric membrane with 300 nm isopores using UV nanoimprint lithography. The highly porous membrane has a pore density of  $4 \times 10^9$  pores per  $\text{cm}^2$  and stable permeance of  $108\,000 \text{ L m}^{-2} \text{ h}^{-1} \text{ bar}^{-1}$ . Uniform ZIF-8 nanoparticles were synthesized and the isoporous membrane successfully demonstrated as high as 100% rejection and size-based sieving performance of nanoparticles.

Received 16th November 2021  
Accepted 22nd December 2021

DOI: 10.1039/d1na00812a

rsc.li/nanoscale-advances

## 1. Introduction

The precise sieving of particles and macromolecules is required in many applications for analytical, diagnostic and preparative purposes.<sup>1–4</sup> After sieving, categorized or isolated samples can be exposed to further diagnosis and individual analysis, for instance, isolating circulation tumor cells (CTCs) from the blood for early detection of cancer disease,<sup>5,6</sup> sorting cells as the enrichment of hematopoietic stem cells for autologous patient treatment,<sup>7</sup> and cell fractionation or organelle sorting for advanced research of their functions and development applications.<sup>8,9</sup> Moreover, sieving is highly in the sterilization of fluids, such as the elimination of bacteria from drinking water,<sup>10</sup> biological and pharmaceutical fluids<sup>11</sup> and for particle elimination from liquids used in microcircuit manufacturing processes.<sup>12</sup>

There are several methods of particle sieving, which have been divided into two groups: active and passive. In the former case, external field force is applied to separate the particles, while passive methods do not utilize external force but rely on inherent characteristics of the particles, such as dimensions, shape and deformability.<sup>13,14</sup> Among the active methods are dielectrophoresis,<sup>15</sup> acoustophoresis,<sup>16</sup> magnetophoresis,<sup>17</sup> optical tweezing<sup>18</sup> and centrifugation,<sup>19</sup> with their efficiency rate

variation between 83 and 92%. However, using active methodologies does not always give accurate performance and one should always be careful since any applied force can damage the separating objects. This can be crucial for particles such as living organisms or cells. Therefore, some biomedical applications require mild conditions in a sieving environment, hence, making passive methods advantageous. The most known methods in the passive group include filtration using porous membranes,<sup>20</sup> a system with pillars<sup>21</sup> or weirs.<sup>22</sup>

Many target species sieved by membranes, *e.g.*, CTCs, blood cells, hepatic cells, and bacteria, have a size range between 0.3 and 12  $\mu\text{m}$ . Isoporous membranes would be ideal for this separation, but practically only track-etched (TE) films are commercially available in this category. However, TE membranes have imperfect uniformity of pore size and distribution with low porosity.<sup>23</sup> We recently reviewed<sup>9</sup> and discussed the existing methodologies to manufacture isoporous polymeric membranes in the lab-scale, where each has drawbacks limiting the performance, application range and suitable materials. As a result, we have successfully presented a new method to fabricate a perfectly uniform, scalable, highly porous polymeric membrane with a large active surface area using advanced nanotechnologies. The methodology we previously demonstrated is solvent and water free and is a combination of photolithography and dry reactive ion etching (RIE) procedures, through which we achieved different isoporous membranes with pore sizes between 0.7 and 50  $\mu\text{m}$ . The fabrication protocol is adaptable to many different homopolymers. However the photolithography/RIE method also has its limitation. It fabricates densely packed pores with a size down to 1  $\mu\text{m}$  (or 0.7  $\mu\text{m}$

<sup>a</sup>King Abdullah University of Science and Technology (KAUST), Biological and Environmental Science and Engineering (BESE) Division, Advanced Membranes and Porous Materials Center, 23955-6900 Thuwal, Saudi Arabia. E-mail: [suzana.nunes@kaust.edu.sa](mailto:suzana.nunes@kaust.edu.sa)

<sup>b</sup>King Abdullah University of Science and Technology (KAUST), Nanofabrication Core Laboratory, 23955-6900 Thuwal, Saudi Arabia



with an additional parylene coating). We have also intensively explored the self-assembly of block copolymers for the preparation of isoporous membranes, which mostly led to pores in the range of 20 to 60 nm.<sup>24</sup> But other approaches have to be developed to provide nanopores with a size below 1  $\mu\text{m}$  applicable to a broader variety of materials, including high performance and stable homopolymers such as poly(ethylene terephthalate) and polyimides.

We found the alternative for isoporous membrane nanofabrication in the recognized solution to the resolution limits of photolithography for intense pattern design, which is nanoimprint lithography (NIL).<sup>25</sup> NIL is one of the advanced nanopatterning methods used to produce semiconductors,<sup>26</sup> hard disk drives,<sup>27</sup> photonics,<sup>28</sup> solar cells,<sup>29</sup> and displays.<sup>30</sup> Recent reports showed the ability to use the technique in biological applications such as tissue engineering,<sup>31</sup> genetic screening<sup>32</sup> and biosensors.<sup>33</sup> Studies by several groups have demonstrated the use of NIL technology to fabricate inorganic porous materials.<sup>34,35</sup> However in the case of organic porous substrates NIL was used only as an assisting step to study the anisotropic nature of polymeric membranes<sup>36</sup> or for enhancement of membrane surface properties.<sup>37,38</sup>

In this work, we present UV nanoimprint lithography (UV-NIL) as nanotechnology to successfully fabricate an isoporous polymeric membrane with high porosity and uniform nanopores with a size down to 300 nm. We use Mylar<sup>®</sup>, a polyester transparent film, known for high chemical and thermal stability.<sup>39</sup> We synthesized uniform ZIF-8 nanoparticles in different sizes to successfully demonstrate the sieving ability of our isoporous membrane.

## 2. Experimental

### 2.1. Materials

Poly(ethylene terephthalate) dense films (Mylar<sup>®</sup>) were purchased from Chemplex Industries, Inc., and 4-inch diameter silicon wafers and glass wafers were bought from University Wafer; cetrimonium bromide (CTAB), zinc acetate dihydrate ( $\text{Zn}(\text{CH}_3\text{COO})_2 \cdot 2\text{H}_2\text{O}$ , >99%) and methylimidazole were supplied by Sigma-Aldrich. All soft stamp materials were provided by EVG: working stamp material UV/AF1 (fluoropolymer), photoinitiator, anti-sticking (methyl fluorobutyl ether) and adhesion agents (isopropyl alcohol). Track-etched membranes were purchased from STERLITECH Corporation, with pore sizes of 400 nm and 200 nm.

### 2.2. Nanoporous membrane fabrication

**2.2.1. Master stamp fabrication.** A pattern with densely distributed 300 nm cylindrical pores and identical 300 nm interpore distance was designed using the Tanner EDA L-Edit software. The GDSII data file of the design was then converted into a machine-exposable file.

A  $\text{SiO}_2$  layer having a thickness of 100 nm was deposited by plasma enhanced chemical vapor deposition (PECVD) using an Oxford Instruments PlasmaLab100. The parameters used for the  $\text{SiO}_2$  deposition were a radio frequency (RF) power of 20 W,

deposition pressure of 1000 mTorr with a gas mixture of  $\text{SiH}_4$  (6 sccm),  $\text{N}_2\text{O}$  (850 sccm) and  $\text{N}_2$  (162 sccm), and a temperature of 300 °C.

The substrate was baked at 180 °C for 10 min followed by an oven vapour priming with hexamethyldisilazane (HDMS) at 150 °C.

200 nm-thick AR-P6200.09 electron-sensitive resists were spin-coated, followed by baking at 150 °C for 3 min.

The pattern was then transferred by exposing the resist with a focused electron beam having an incident energy of 100 kV, generated by the electron beam (e-beam) lithography tool (JEOL JBX - 6300FS). The base dose used for exposure was 190  $\mu\text{C cm}^{-2}$ , having a maximum stage moving speed of 50 MHz.

After the electron irradiation, the sample was developed using AR 600-546 (Allresist GmbH) for 1 min, then dipped for 5 s in oxylene (Alfa Aesar), rinsed with DI water for 30 s and heated at 130 °C for 1 min.

To etch out the  $\text{SiO}_2$  sacrificial layer first, the substrate was loaded into the Inductively Coupled Plasma (ICP) – Reactive Ion Etcher (RIE) tool (Oxford Instruments PlasmaLab100). The used parameters were a RF power of 100 W, ICP power of 1500 W, chamber pressure of 10 mTorr and gas mixtures of  $\text{C}_4\text{F}_8$  (40 sccm) and  $\text{O}_2$  (5 sccm), at 10 °C.

Finally, the Si wafer was etched using the same ICP-RIE tool with the process cycle consisting of one deposition and one etching step parameters: the ICP power of 1300 W, chamber pressure of 30 mTorr, and a temperature of 10 °C. The gas mixture used for the deposition step was  $\text{C}_4\text{F}_8$  (100 sccm) and  $\text{SF}_6$  (10 sccm), at an RF power of 5 W for 5 s, while for the etch step the gas mixture was  $\text{C}_4\text{F}_8$  (10 sccm) and  $\text{SF}_6$  (100 sccm) at an RF power of 30 W for 9 s. Keeping the parameters constant, the cycles were repeated until a depth of about 2  $\mu\text{m}$  was obtained.

The master stamp was then washed with acetone/IPA and dried with nitrogen.

**2.2.2. Soft stamp fabrication.** To make a soft stamp or poly(dimethyl siloxane) (PDMS) mold out of the fabricated silicon master stamp, we prepared the PDMS solution by mixing 10 mL of working stamp material UV/AF1 (fluoropolymer) with 2.5 mL of photoinitiator and left it stirring overnight. A thin anti-sticking layer (methyl fluorobutyl ether) was applied to the master stamp by spin-coating, followed by baking at 120 °C for 10 minutes and cooling down for a minute. A glass wafer, served as a soft stamp base, was first dehydrated at 200 °C for 5 minutes, coated with an adhesion layer (isopropyl alcohol) and baked for 2 minutes at 120 °C. After preparing the samples, the master and glass stamps were fixed with vacuum on two separate stamp plates. Then the PDMS solution was poured slowly on top of the master stamp and the glass wafer plate was merged or “sandwiched” on top of it. The system was exposed to UV light (16  $\text{mW cm}^{-2}$ ) and cured for an hour. The patterned soft stamp was accurately detached from the master stamp. The master stamp was cleaned with  $\text{O}_2$  plasma for any next reuse.

**2.2.3. Membrane fixture fabrication.** The membrane fixture, such as embroidery hoops, has 2 parts which were built from two thick silicon wafers, as shown in Fig. 1(b). They were fabricated by photolithography and dry RIE procedures. The base wafer was etched with a UV-exposed negative photoresist



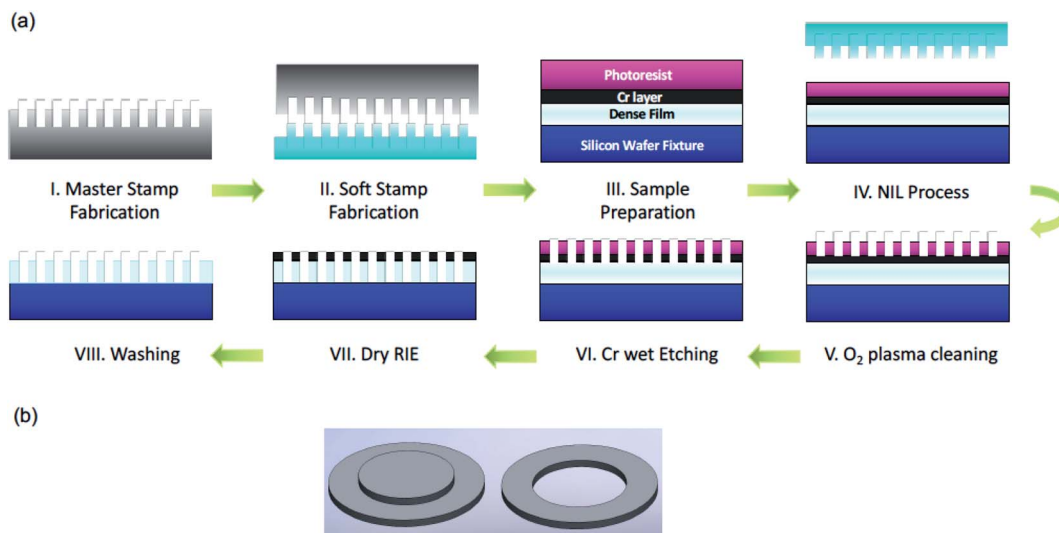


Fig. 1 (a) NIL process step illustration; (b) silicon fixture 3D representation.

and the top wafer with a positive photoresist, both from a photomask with a circular pattern (60 mm in diameter). The Mylar<sup>®</sup> film is placed in between the two fixture parts which were clamped with magnets.

**2.2.4. Chromium deposition.** The Mylar<sup>®</sup> dense film was first coated with 30 nm of Cr thin film using a reactive sputter deposition tool (Equipment Support Company).

**2.2.5. Nanoimprint lithography (NIL).** The Cr coated film was secured in the fixture, then was coated with an adhesion promoter and then with 200 nm of UV/A2 photoresist (ethyl-(L)-lactate) followed by baking at 120 °C for a minute. After that, the patterned soft stamp and the membrane system were both loaded into the nano-imprint photolithography tool (EVG-620). The soft stamp and the membrane system were aligned and pressed together with a total pressure of 950 mbar, applied gradually with a 50 mbar increase step. Next, it was exposed under a 180 mJ cm<sup>-2</sup> of UV light for 200 seconds. After the exposure, the system was applied to the O<sub>2</sub> plasma cleaning procedure.

**2.2.6. Wet-etching.** Before the dry reactive ion etching process, the patterned membrane system was immersed into chromium etchant (TechniEtch Cr01) for 30 seconds. It was then rinsed with DI water and dried under nitrogen.

**2.2.7. Dry-etching.** The patterned pores were finely etched out with a dry-etching process, using an inductive-coupled plasma reactive ion etching (ICP-RIE) instrument (Oxford Instruments), with the following parameters: a sulfur hexafluoride (SF<sub>6</sub>) flow of 10 standard-cubic centimeters per minute (sccm) and oxygen (O<sub>2</sub>) flow of 30 sccm, a pressure of 8 mTorr, RF power of 25 W, and ICP power of 600 W. The etching process was performed in 3 steps for 9 minutes. The final product was washed with acetone and isopropyl alcohol and rinsed with DI water. The nanoporous membrane was then easily detached from the fixture.

### 2.3. Membrane characterization

**2.3.1. Surface morphology.** The nanoporous membrane, as well as ZIF-8 nanoparticles, was imaged by scanning electron

microscopy (SEM) on a Quanta 3D FEI microscope. Before imaging, the membrane samples were sputter-coated with a 4 nm thick layer of iridium, analogously to the ZIF-8 nanoparticles, which were first attached and dried on a piece of silicon wafer.

**2.3.2. ZIF-8 particle preparation for the rejection test.** Zn(CH<sub>3</sub>COO)<sub>2</sub>·2H<sub>2</sub>O (3 g, 0.27 M) was dissolved in DI water (50 mL). In a separate container, the CTAB surfactant (331.6 mg, 1.8 mM) was dissolved in DI water (414.5 g) by stirring for 3 hours. In a third container, methylimidazole (15.6 g, 3.8 M) was dissolved in 50 mL solution of DI water mixed with the surfactant solution. Then, the mixture was poured rapidly into the first container, stirred for 15 seconds and was left for 2 hours at room temperature to generate the ZIF-8 nanoparticles. After that, the final solution was distributed in several tubes and centrifugated at 5000 rpm for 11 minutes. Finally, the sedimented particles were washed with DI water and centrifuged again, followed by two more similar washing procedures.

## 3. Results and discussion

### 3.1. Membrane fabrication

The fabrication process starts by manufacturing the master stamp, as shown in Fig. 1(a). The design containing up to half a billion of 300 nm isopores with an identical interpore distance was transferred *via* e-beam lithography onto a 4-inch Si wafer which was first cleaned then deposited with the sacrificial hard mask of silicon dioxide and coated with the positive electron sensitive resist. Finally, the cavities in the master stamp were etched out with two procedures using the ICP DRIE tool. The reusable master stamp with 300 nm diameter cavities was used to create a soft stamp with 300 nm pillars by curing the PDMS solution on it *via* UV. Both, Si master stamp and PDMS soft stamp, were imaged by atomic force microscopy (AFM), as shown in Fig. 2a and b. Then, a 2.5 μm thick Mylar<sup>®</sup> film, as a base material, was first coated with a Cr protective layer and



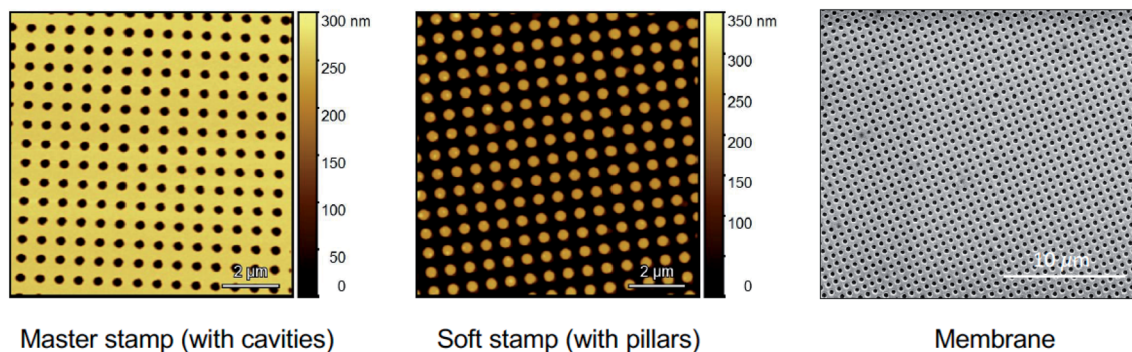


Fig. 2 (a and b) AFM images of the (a) master stamp and (b) soft stamp; (c) SEM images of the membrane fabricated *via* NIL.

then fixed within the specially fabricated fixture, as illustrated in Fig. 1(b), in order to achieve a very smooth surface without any glueing material. The photoresist coated membrane system was exposed to the soft stamp through UV in the photolithographic set-up. After the oxygen cleaning and wet-etching process, the nanopores were then etched out by the dry etching procedure. In the end, the nanoporous membrane, easily extracted from the fixture, was cleaned and dried.

### 3.2. Membrane characterization

The obtained nanoporous membrane surface was imaged by scanning electron microscopy (SEM), as shown in Fig. 2c. Highly ordered 300 nm nanopores with a similar inter-pore space led to a density of  $4 \times 10^9$  pores per  $\text{cm}^2$ .

The membrane permeance and rejection of particles with different sizes were investigated, as shown in Fig. 3. The water permeance measurement was performed using a stainless-steel filtration cell with an active membrane area of  $1 \text{ cm}^2$ , a water feed volume of 300 mL and a trans-membrane pressure of 0.03 bar. A stable water permeance of  $108\,000 \text{ L m}^{-2} \text{ h}^{-1} \text{ bar}^{-1}$  was measured, as shown in Fig. 3d, which is *ca.* 3 to 13-fold higher than the permeation value of  $38\,000 \text{ L m}^{-2} \text{ h}^{-1} \text{ bar}^{-1}$  and  $8500 \text{ L m}^{-2} \text{ h}^{-1} \text{ bar}^{-1}$  obtained with the track-etched membranes with pore sizes of 400 nm and 200 nm, respectively.

In order to check the membrane rejection performance, homogeneous zeolitic imidazolate framework (ZIF) nanoparticles were synthesized with sizes of 200 nm, 400 nm and 600 nm. The ZIF-8 nanoparticle sizes were controlled by the

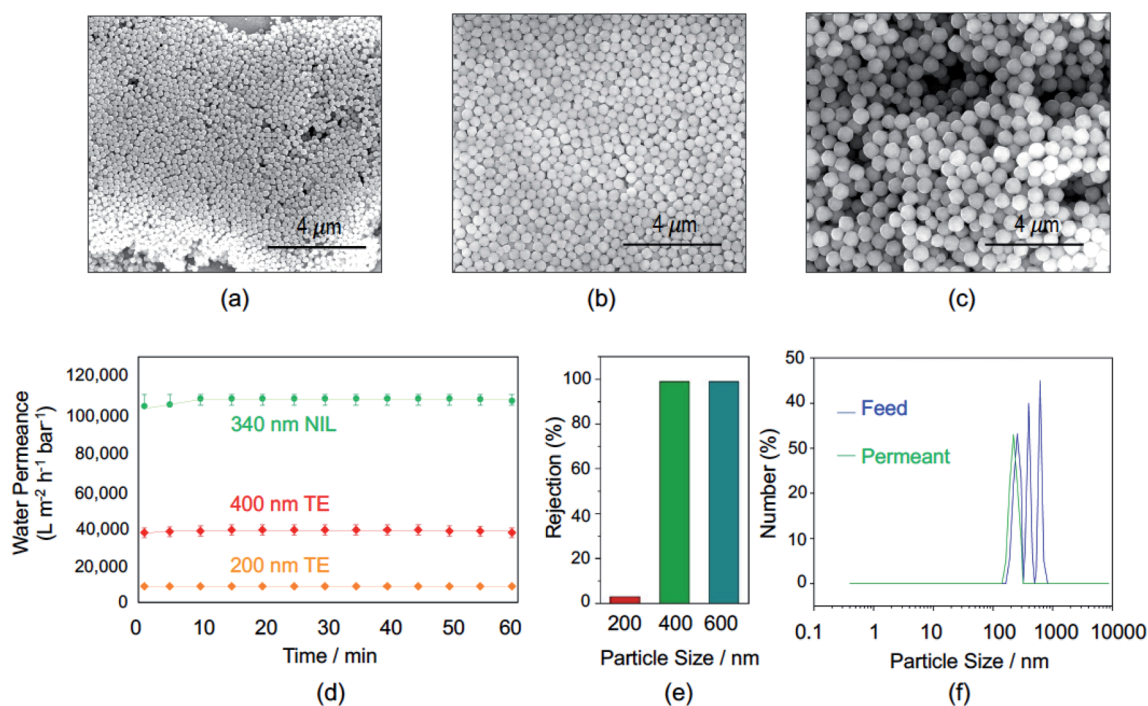


Fig. 3 (a–c) SEM images of homogeneous ZIF-8 nanoparticles with diameters of (a) 200 nm, (b) 400 nm and (c) 600 nm; (d) water permeance of NIL and TE membranes; (e) nanoparticle rejection by the 340 nm porous NIL membranes; (f) DLS graph of mixed nanoparticles in the feed and permeant in tests with NIL membranes.



surfactant amount added. To synthesize 200 nm sized nanoparticles, 15 mL of CTAB solution was added, while 400 nm and 600 nm nanoparticles were generated with 7 mL and 1.5 mL, respectively. Fig. 3(a–c) show the SEM images of ZIF-8 nanoparticles in different sizes.

The rejection tests were performed using dialysis glass cells. ZIF-8 nanoparticles with three different sizes were diluted in DI water separately as homogeneous mixtures and rejection tests were first performed in three separated cells. Then, a cell was used to test the sieving performance of the membrane using a heterogeneous solution with mixed 200 nm, 400 nm and 600 nm ZIF-8 nanoparticles. To see the rejection results, the feed and permeate solutions were analysed by dynamic light scattering (DLS). The graphs are shown in Fig. 3(e and f). The rejection efficiency for 400 nm and 600 nm ZIF-8 nanoparticles were as high as 100%, while for 200 nm nanoparticles it was only 3%; the membrane provides a sharp fractionation of particles in the investigated size range (Fig. 3f).

## 4. Conclusions

We have developed a new fabrication protocol for manufacturing an isoporous polymeric membrane with 300 nm uniform nanopores using UV-NIL, a technique combining nanopatterning and dry reactive ion etching processes. The fabricated hard master and soft PDMS stamps are reusable. The high sieving performance of the nanofabricated isoporous membrane has been demonstrated with synthesized uniform ZIF-8 nanoparticles of different sizes. The membrane with strong chemical and thermal resistances is flexible, transparent and thin (2.5  $\mu\text{m}$ ) making it advantageous for integration into a microfluidic device and examination of samples by optical microscopy.

## Author contributions

A. S. developed the membranes and performed the characterization studies. C. F. F., F. P. J., A. S. D. and U. B. assisted in the nanofabrication experiments. X. L. assisted in the nanoparticle preparation. S. P. N. supervised the project. A. S. and S. P. N. wrote the first version of the paper, which was then revised by all authors.

## Conflicts of interest

The authors declare no competing interests.

## Acknowledgements

This work was supported by the King Abdullah University of Science and Technology (KAUST).

## References

- 1 F. Lyu, M. Thomas, W. Hendriks and A. Van der Poel, *Anim. Feed Sci. Technol.*, 2020, **261**, 114347.
- 2 A. S. Shanbhag, J. J. Jacobs, J. Black, J. O. Galante and T. T. Glant, *J. Biomed. Mater. Res.*, 1994, **28**, 81–90.
- 3 F. Fan and K. J. Stebe, *Langmuir*, 2005, **21**, 1149–1152.
- 4 S. Wustoni, S. Wang, J. R. Alvarez, T. C. Hidalgo, S. P. Nunes and S. Inal, *Biosens. Bioelectron.*, 2019, **143**, 111561.
- 5 S. Zheng, H. Lin, J.-Q. Liu, M. Balic, R. Datar, R. J. Cote and Y.-C. Tai, *J. Chromatogr. A*, 2007, **1162**, 154–161.
- 6 S.-J. Hao, Y. Wan, Y.-Q. Xia, X. Zou and S.-Y. Zheng, *Adv. Drug Delivery Rev.*, 2018, **125**, 3–20.
- 7 M. J. Tomlinson, S. Tomlinson, X. B. Yang and J. Kirkham, *J. Tissue Eng.*, 2013, **4**, 2041731412472690.
- 8 J. S. Yang, J. Y. Lee and M. H. Moon, *Anal. Chem.*, 2015, **87**, 6342–6348.
- 9 A. Sabirova, F. Pisig, N. Rayapuram, H. Hirt and S. P. Nunes, *Sci. Rep.*, 2020, **10**, 1–9.
- 10 L. Clime, X. D. Hoa, N. Corneau, K. J. Morton, C. Luebbert, M. Mounier, D. Brassard, M. Geissler, S. Bidawid and J. Farber, *Biomed. Microdevices*, 2015, **17**, 1–14.
- 11 H. Aranha-Creado, in *Biotechnology*, ed. C. M. W. V. L. W. K. E. Avis, CRC Press, 2020, ch. 4, pp. 167–219.
- 12 D. W. Cooper, *Aerosol Sci. Technol.*, 1986, **5**, 287–299.
- 13 M. Li, H. E. Muñoz, K. Goda and D. Di Carlo, *Sci. Rep.*, 2017, **7**, 1–8.
- 14 E. S. Park, C. Jin, Q. Guo, R. R. Ang, S. P. Duffy, K. Matthews, A. Azad, H. Abdi, T. Todenhöfer and J. Bazov, *Small*, 2016, **12**, 1909–1919.
- 15 H. Shafiee, M. B. Sano, E. A. Henslee, J. L. Caldwell and R. V. Davalos, *Lab Chip*, 2010, **10**, 438–445.
- 16 T. Laurell, F. Petersson and A. Nilsson, *Chem. Soc. Rev.*, 2007, **36**, 492–506.
- 17 D. Robert, N. Pamme, H. Conjeaud, F. Gazeau, A. Iles and C. Wilhelm, *Lab Chip*, 2011, **11**, 1902–1910.
- 18 B. Landenberger, H. Höfemmann, S. Wadle and A. Rohrbach, *Lab Chip*, 2012, **12**, 3177–3183.
- 19 T. Morijiri, S. Sunahiro, M. Senaha, M. Yamada and M. Seki, *Microfluid. Nanofluid.*, 2011, **11**, 105–110.
- 20 X. Li, W. Chen, G. Liu, W. Lu and J. Fu, *Lab Chip*, 2014, **14**, 2565–2575.
- 21 J. Alvankarian, A. Bahadorimehr and B. Yeop Majlis, *Biomicrofluidics*, 2013, **7**, 014102.
- 22 P. Wilding, L. J. Kricka, J. Cheng, G. Hvichia, M. A. Shoffner and P. Fortina, *Anal. Biochem.*, 1998, **257**, 95–100.
- 23 V. Ramachandran and H. S. Fogler, *J. Fluid Mech.*, 1999, **385**, 129–156.
- 24 S. P. Nunes, *Macromolecules*, 2016, **49**, 2905–2916.
- 25 M. C. Traub, W. Longsine and V. N. Truskett, *Annu. Rev. Chem. Biomol. Eng.*, 2016, **7**, 583–604.
- 26 S. Sreenivasan, *Microsyst. Nanoeng.*, 2017, **3**, 1–19.
- 27 T. Glinsner, P. Hangweier, H. Luesebrink, P. Dorsey, A. Homola and D. Wachenschwanz, *Solid State Technol.*, 2005, **48**, 51–54.
- 28 S. H. Kim, K.-D. Lee, J.-Y. Kim, M.-K. Kwon and S.-J. Park, *Nanotechnology*, 2007, **18**, 055306.
- 29 C. Battaglia, J. Escarré, K. Söderström, L. Erni, L. Ding, G. Bugnon, A. Billet, M. Boccard, L. Barraud and S. De Wolf, *Nano Lett.*, 2011, **11**, 661–665.



- 30 E.-H. Cho, H.-S. Kim, J.-S. Sohn, C.-Y. Moon, N.-C. Park and Y.-P. Park, *Opt. Express*, 2010, **18**, 27712–27722.
- 31 K. Li, K. Morton, T. Veres, B. Cui and M. Murray, in *Comprehensive Biotechnology*, Citeseer, 2011, pp. 125–139.
- 32 D. Xia, J. Yan and S. Hou, *Small*, 2012, **8**, 2787–2801.
- 33 C.-C. Yu, K.-H. Ho, H.-L. Chen, S.-Y. Chuang, S.-C. Tseng and W.-F. Su, *Biosens. Bioelectron.*, 2012, **33**, 267–273.
- 34 J. D. Ryckman, Y. Jiao and S. M. Weiss, *Sci. Rep.*, 2013, **3**, 1–7.
- 35 K. Imakita, T. Kamada, M. Fujii, K. Aoki, M. Mizuhata and S. Hayashi, *Opt. Lett.*, 2013, **38**, 5067–5070.
- 36 S. H. Maruf, Z. Li, J. A. Yoshimura, J. Xiao, A. R. Greenberg and Y. Ding, *Polymer*, 2015, **69**, 129–137.
- 37 S. T. Weinman and S. M. Husson, *J. Membr. Sci.*, 2016, **513**, 146–154.
- 38 Z. Ma, S. Liang, K. Xiao, X. Wang, M. Li and X. Huang, *J. Membr. Sci.*, 2020, **612**, 118332.
- 39 L. E. Amborski and D. W. Flierl, *Ind. Eng. Chem.*, 1953, **45**, 2290–2295.

